第33卷 第4期 焊 接 学 报 Vol. 33 No. 4
2012年4月 TRANSACTIONS OF THE CHINA WELDING INSTITUTION April 2012

脉冲逆变焊接电源建模与仿真

段 彬[1]， 张承慧[1]， 孙同景[1]， 张光先[2]， 郭 民[1]
(1. 山东大学 控制科学与工程学院，济南 250061;
2. 山东奥太电气有限公司，济南 250000)

段 彬

摘 要：构建了包含输入、输出整流滤波和逆变、降压等电路的物理模型，通过非线性接口模型，研究了主回路和数字控制系统的整体建模与仿真. 建立了动态焊接过程的系统数学模型，利用 Matlab 对焊接电源系统进行了仿真研究，然后定量分析了扰动作用下各物理量变化规律和系统动态响应过程，有效预测了脉冲 MIG 焊接电源的工作过程，指出了焊接电流和电弧电压控制的意义，为进一步研究指明了方向.

关键词：逆变焊接电源；脉冲焊；数学建模；仿真
中图分类号：TG409 **文献标识码**：A **文章编号**：0253－360X(2012)04－0057－04

0 序 言

逆变弧焊电源数字控制技术的关键在于系统硬件结构设计和算法的软件实现，这两部分工作都要求全面的分析和了解被控对象与控制系统，所以有必要对系统进行建模、仿真和分析. 弱电与强电结合的逆变焊接电源本质为非线性系统，其工作环境恶劣，而且功率器件价格昂贵并极易损坏，因此仿真研究显得尤为重要. 焊接过程的仿真得到了国际焊接界的高度重视[1]. 美国焊接学会认为焊接过程仿真是未来焊接技术发展的关键驱动力. 与普通恒流焊接方式不同，脉冲 MIG 焊控制参数和影响因素较多，而计算机仿真技术不仅可对焊接工艺参数和焊接效果进行预测，还可对主回路和控制回路的设计及新控制方法的研究进行指导，具有方便、成本低、安全性好、研制周期短等许多优点.

目前焊接动态过程的计算机仿真研究已有许多，但针对 CO_2 气保焊短路熔滴过渡过程的研究居多[2]，而脉冲 MIG 焊接技术的仿真研究较少. 为减少盲目性提高研究效率，文中以脉冲 MIG 焊为研究对象，提出物理模型和数学模型相结合的新方法，以交互式编程软件 Matlab 为工具，研究数字脉冲 MIG 焊接电源系统的特点及其参数变化的动态响应过程，为控制策略的研究和系统设计指明方向.

收稿日期：2011－03－02
基金项目：山东大学自主创新基金资助项目(2010GN067)；济南青年科技明星计划资助项目(20110304)

1 主回路物理模型建立与仿真

1.1 主回路物理模型

逆变弧焊电源系统结构如图 1 所示. 目前多采用金属氧化物半导体场效应管(MOSFET)或 Switch 模型代替绝缘栅双极型晶体管(IGBT)[3]. 为最大程度逼近实际，文中采用 IGBT 和二极管的并联结构进行仿真研究.

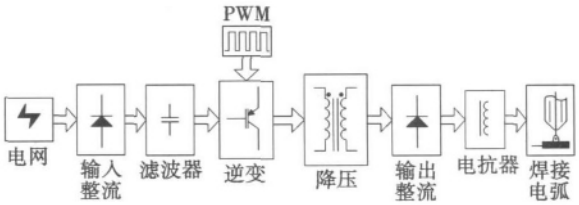

图 1 数字脉冲 MIG 焊接电源系统结构

Fig. 1 Functional block of full digital pulse MIG welding power source

根据设计的焊接电源样机结构及选用的各元器件厂家、类型、工艺等信息，设置仿真参数. 图 2 为全桥硬开关结构，由 4 路 PWM 脉冲驱动，变压器变比为 20∶4，逆变频率为 30 kHz. D5 和 D6 构成全波整流器. 经输出电抗供电由电阻模拟的电弧负载.

1.2 仿真验证与分析

构建数字脉冲逆变焊接电源电流闭环系统模型，如图 3 所示，包含电源输入模型、主回路模型、电弧负载等效电阻、采样保持延时环节、给定电流发生

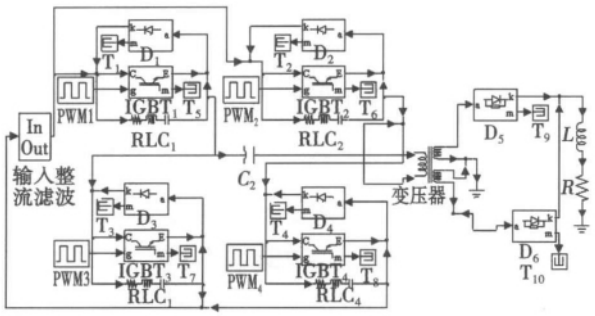

图 2 脉冲逆变焊接电源主回路仿真模型

Fig. 2 Simulation model of main loop circuit

器、PID 控制器和 PWM 发生器 7 个部分，其中 I_f 为焊接电流，I_o 为变压器原边电流，K_p，K_i 为比例系数和积分系数.

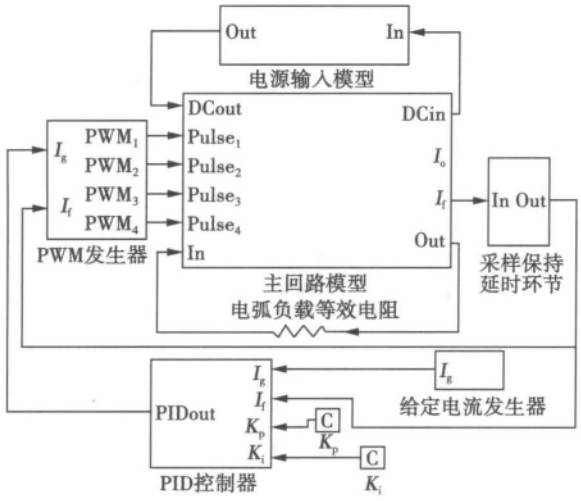

图 3 焊接电流闭环仿真

Fig. 3 Simulation of welding current loop

给定电流发生器(given current generator)产生 250 Hz 的方波电流，其峰值、基值大小分别为 500 A 和 100 A，占空比为 50%. 图 4 为电流响应曲线，

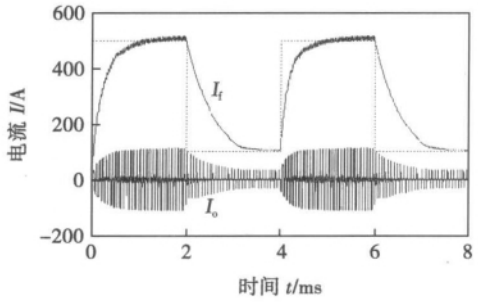

图 4 焊接电流响应图

Fig. 4 Current waveform

图 5 为图 4 电流上升段展开波形. 控制算法实时调节 PWM 驱动脉冲的占空比逐渐减小，直至 I_f 达到电流给定 I_g. 由于电感器的存在，I_f 有较小的纹波，且输出电抗值越大，纹波的波动越小，但这也会同时降低了系统的响应速率.

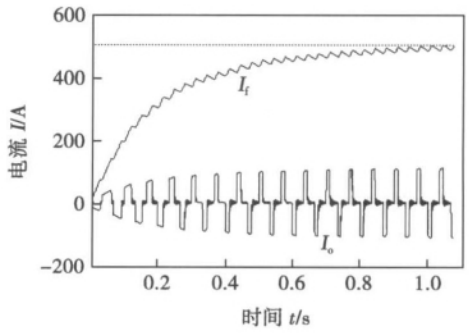

图 5 焊接电流波形展开图

Fig. 5 Current extension

2 逆变焊接电源系统建模与仿真

2.1 主回路数学模型

首先作以下假设: 由于回路电感相对输出电抗器电感值很小，忽略导线等产生的回路电感; 由于弧长相对熔滴直径较长，忽略熔滴体积的影响; 同时忽略高频变压器漏感和熔池平面振荡对弧长的影响，得到图 6 脉冲 MIG 焊接电源等效示意图，其中 R 为焊接回路等效电阻，包含焊接回路导线和焊接电缆的电阻、焊丝和导电嘴的接触电阻等，L 为输出电抗器的电感值; v_f 为送丝速度; v_m 为焊丝熔化速度. 反馈电压 U_f 通常取自焊枪，可认为是焊丝伸出长度电压 U_e 和电弧电压 U_a 之和. l_e 为焊丝伸出长度; l_a 为电弧长度.

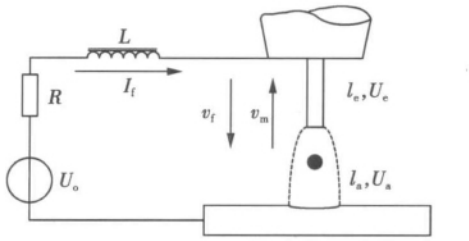

图 6 脉冲 MIG 焊接电源等效示意图

Fig. 6 Equivalent diagram of PMIG welding power source

将逆变电源主回路中的输入整流滤波环节、逆变环节以及输出整流环节等价为电源等效输出电压，即

$$U_o = \frac{U_{DC}D}{n} \tag{1}$$

式中: U_{DC} 为直流母线电压; D 为占空比; n 为主变压器匝数比. 根据戴维宁定理得

$$U_o = I_f R + L\frac{dI_f}{dt} + U_e + U_a \tag{2}$$

利用拉普拉斯变换得

$$U_o(s) = U_a(s) + U_e(s) + I_f(s)R(s) + sLI_f(s) \tag{3}$$

结合式(1) ~式(3),得到输入为 D,U_a 和 U_e,输出为 I_f 的主回路模型.

2.2　脉冲 MIG 焊接电弧模型

脉冲 MIG 焊采用惰性气体为保护气,常为喷射过渡方式. 电弧是非线性负载,其电压受电流、弧长、保护气体和电极材料等诸多因素影响. 目前国内外许多研究人员对焊接电弧特性进行了多年研究和大量试验,其中 Muller 等人的试验结果被认为是最贴近实际的[8],如图 7 所示,图 7a 是氩气保护下使用直径为 2.4 mm 铝焊丝时的电弧静特性曲线,它表明弧长一定时,MIG 焊电弧电压随焊接电流增大而增大,这也是 MIG 电弧的独特之处; 图 7b 表明 MIG 电弧电压与弧长近似成正比关系.

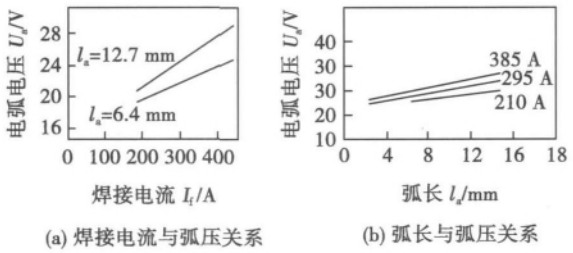

图 7　电弧电压与焊接电流及电弧弧长的关系

Fig. 7　Curves of arc voltage, welding current and arc length

由电弧物理知,在焊丝材料、直径等因素确定后,忽略阳极电压 U_A 和阴极电压 U_K 的微小变化,U_a 可认为是 I_f 和电弧长度 l_a 的函数,因此式(4) 可近似作为电弧电压模型,k_1,k_2 和 k_3 为常系数.

$$U_a = f(I_f, l_a) = k_1 + k_2 I_f + k_3 l_a \tag{4}$$

2.3　焊丝伸出长度压降模型分析

根据电阻公式,得焊丝伸出长度电阻为

$$R_e = \frac{\eta l_e}{S} \tag{5}$$

式中: S 为焊丝横截面积; η 是与焊丝材料有关的电阻率,与温度成正比,即

$$\eta = \eta_0 \times (1 + a_0 T) \tag{6}$$

式中: η_0 为 0 ℃时的电阻率; a_0 为平均温度系数; T 为当前温度. 由于焊丝伸出长度各处温度不同,难以精确获取实际温度,计算电阻. 根据测试材料的特性,估计平均温度,得到以伸出长度平均温度和变化的 l_e,I_f 为输入,输出为 U_e 的伸出长度压降模型.

2.4　焊丝熔化速度模型

高温下焊丝熔化的热量来自电弧热 H_a 和电阻热 H_L 两部分. 傅希圣等人[5-7] 建立的焊丝熔化速度半理论公式为

$$v_m = f(l_e, I_f) = \frac{1}{H_0 + b}(al_e j^2 + \phi j) \tag{7}$$

$$j = \frac{I_f}{S} = \frac{I_f}{\pi(d/2)^2} \tag{8}$$

式中: a 为焊丝比电阻; b 为 H_L 的函数曲线截距; j 为电流密度; ϕ 为阳极等效电压; H_0 为熔滴单位体积热焓,d 为焊丝直径.

v_m 主要取决于 l_e 和 I_f,与 l_a 几乎无关,因此当 I_f 恒定时,只要 l_e 确定,无论 l_a 如何变化,v_m 基本恒定. 焊接过程中,由于 l_a 极易波动,必须调节 l_e,维持 l_a 稳定. 当平衡状态被打破,得焊丝伸出长度变化率的微分方程为

$$\frac{dl_e}{dt} = v_f - v_m \tag{9}$$

由式(7) 和式(9) 得

$$v_f - \frac{dl_e}{dt} = \frac{1}{H_o + b}(al_e j^2 + \phi j) \tag{10}$$

2.5　系统整体模型

图 8 为脉冲逆变焊接电源整体模型,其中采样保持延时环节实现模拟系统与数字控制系统的接口,不断采集反馈电压 $U_{feedback}$ 送至电弧控制系统. 通过弧压控制环节调节 $U_{feedback}$,使之稳定在 U_g 大小,并把电流波形参数送给波形发生器,自动调节焊接电流波形,实现弧压的实时控制.

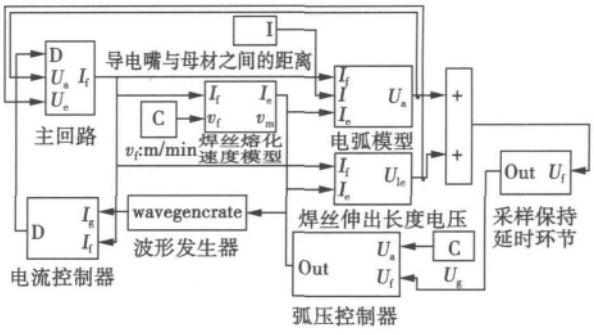

图 8　脉冲 MIG 焊接电源系统仿真模型

Fig. 8　Simulation model of system

3 仿真与分析

文中设计了焊枪抖动或工件坡度造成导电嘴与母材之间的距离 l 变化这一常见干扰，来分析电弧、送丝、焊丝熔化和控制等系统间的相互影响，研究电弧动态变化行为. 以 d 为 1.0 mm 的碳钢为例，v_f 为 6 m/min，R 为 0.002 Ω，b 和 H_0 分别为 5.0，12.36 J/mm^3，其它仿真参数如表 1 所示. 在 4 s 时刻，l 由 30 mm 变化到 35 mm.

表 1 仿真试验参数

Table 1 Simulation parameters

给定电压 U_g/V	输出电感 L/μH	焊丝比电阻 a/(10^{-5}Ω·mm)	阳极等效电压 ϕ/V
28	40	130	5.20

当 l 突然增大，l_a 变大，导致 U_a 变大，如图 9 所示. 比较图 10 与图 9，$U_{feedback}$ 与 U_a 的响应曲线类同，U_e 对弧压控制的影响很小. 图 11 表明由于 l 突变，导致 l_a 变长，则控制系统将调节平均焊接电流减小，使 $v_m < v_f$，l_e 逐渐变长，l_a 恢复到原稳定长度.

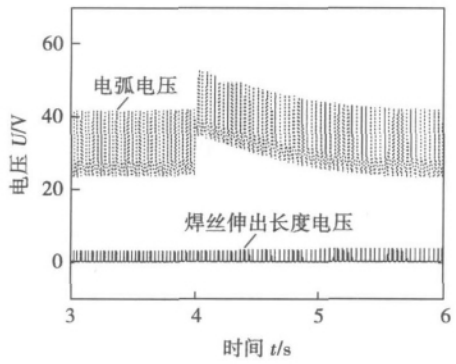

图 9 U_a 和 U_e 的动态响应曲线

Fig. 9 Dynamic response curves of U_a and U_e

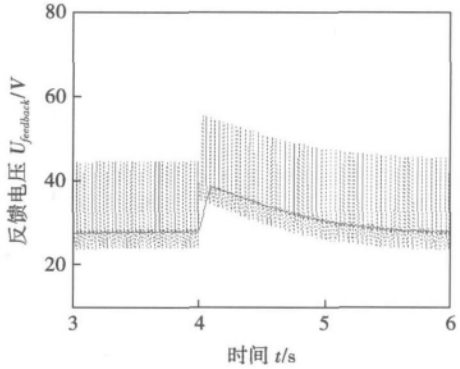

图 10 $U_{feedback}$ 动态响应曲线

Fig. 10 Dynamic curve of $U_{feedback}$

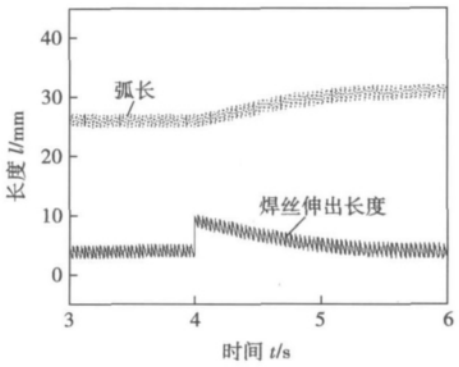

图 11 l_a 和 l_e 变化曲线

Fig. 11 Curves of l_a and l_e

弧长的调节过程，本质是 v_m 的调节，现象是 l_e 的变化，可控参数为平均电流值，而可调节的参数较多，有峰值、基值电流大小和时间、上升和下降速率、脉冲频率等参数.

4 结 论

(1) 首次研究了脉冲逆变焊接电源的整体建模与仿真，对搭建焊接主回路平台，以及研究主回路与控制系统的关系具有重要的指导作用.

(2) 利用建立的动态数学模型，通过干扰因素的引入和定量分析，充分认识了脉冲 MIG 焊接过程中各物理量变化机理和相关参数的影响，指出了焊接电流和电弧电压闭环控制的意义，为控制策略的研究提供了参考依据.

参考文献:

[1] 尹登科，童彦刚，杨晓峰. 计算机仿真技术在数字化焊机电源中的应用[J]. 电焊机，2008，38(11)：59－62.
Yin Dengke，Tong Yangang，Yang Xiaofeng. Application of computer simulation to digital welding power source [J]. Electric Welding Machine，2008，38(11)：59－62.

[2] 罗 怡，许先果. CO_2 焊接电源－电弧系统动态特性的仿真及试验[J]. 焊接技术，2005，34(1)：38－40.
Luo Yi，Xu Xianguo. The dynamic simulation and test of CO_2 arc welding power supply and arc system [J]. Welding Technology，2005，34(1)：38－40.

[3] 张光先，邹增大，陈仁富，等. CO_2 气保焊表面张力过渡的建模及仿真[J]. 焊接学报，2003，24(4)：68－72.
Zhang Guangxian，Zou Zengda，Chen Renfu，*et al*. Modeling and simulation of the CO_2 gas shielded welding surface tension transition [J]. Transactions of the China Welding Institution，2003，24(4)：68－72.

[下转第 64 页]

层,接头多断裂于界面处,为脆性断裂.

参考文献:

[1] 任德亮,齐海波,丁占来,等. SiC 颗粒增强铝基复合材料的焊接[J]. 焊接技术,1999(3):10-12.
Ren Deliang, Qi Haibo, Ding Zhanlai, *et al*. SiC particle reinforced aluminum matrix composite welding [J]. Welding Technology, 1999(3): 10-12.

[2] 刘黎明,祝美丽,徐卫平,等. 铝基复合材料 SiC_w/6061Al 的激光焊接[J]. 焊接学报,2001,22(4):13-16.
Liu Liming, Zhu Meili, Xu Weiping, *et al*. Laser welding SiC_w/6061Al composite [J]. Transactions of the China Welding Institution, 2001, 22(4): 13-16.

[3] 方 玲,张小联,陈康华. 高体积分数 SiC_p/Al 复合材料的细观结构设计及性能研究[J]. 稀有金属与硬质合金,2009,37(2):22-25.
Fang Ling, Zhang Xiaolian, Chen Kanghua. Meso-structure design of high-volume-fraction SiC_p/Al composites and their properties [J]. Rare Metals and Cemented Carbides, 2009, 37(2): 22-25.

[4] 牛济泰,刘黎明,孟庆昌,等. Al_2O_{3p}/6061Al 复合材料焊接工艺参数的优化及接头组织[J]. 焊接学报,1999,20(1):28-32.
Niu Jitai, Liu Liming, Meng Qingchang, *et al*. Optimization of welding parameters and microstructure of welded Joint of Al_2O_{3p}/6061Al composite [J]. Transactions of the China Welding Institution, 1999, 20(1): 28-32.

[5] 夏德顺. 铝基复合材料焊接研究述评[J]. 导弹与航天运载技术,1999(6):38-46.
Xia Deshun. Review of aluminum matrix composite welding [J]. Missiles and Space Vehicles, 1999(6): 38-46.

[6] 牛济泰,吴 林,张德库,等. 铝基复合材料的焊接新工艺[C]// 第十一次全国焊接会议论文集(第1册). 上海,2005:245-248.

[7] 陈彦宾,张德库,牛济泰,等. 激光焊接铝基复合材料的原位增强作用[J]. 应用激光,2002,22(3):320-338.
Chen Yanbin, Zhang Deku, Niu Jitai, *et al*. In-situ reinforcing effect of Ti on aluminum matrix composite during laser beam welding [J]. Appled Laser, 2002, 22(3): 320-338.

作者简介: 李俐群,女,1970 年出生,教授,博士研究生导师. 主要从事先进材料的激光焊接技术、激光表面改性研究. 发表论文 100 余篇. Email: liliqun@hit.edu.cn

[上接第 60 页]

[4] 安藤弘平. 焊接电弧现象[M]. 北京:机械工业出版社,1985.

[5] 傅希圣,牛尾诚夫. MAG 焊时焊丝熔化速度与送丝速度稳定平衡的物理本质[J]. 焊接技术,1997,10(3):2-5.
Fu Xisheng, Mu Shio. The physical nature of wire melting speed and feeding speed stable equilibrium of MAG welding [J]. Welding Technology, 1997, 10(3): 2-5.

[6] 傅希圣,李 烨. 焊丝熔化率公式研究[J]. 焊接学报,1995,16(4):226-231.
Fu Xisheng, Li Ye. Formula of wire melting rate [J]. Transactions of the China Welding Institution, 1995, 16(4): 226-231.

[7] 傅希圣,李 烨,王夏冰. 熔化极气体保护焊焊丝伸出长度和电弧弧长的稳定性. 焊接学报[J],1995,16(2):100-104.
Fu Xisheng, Li Ye, Wang Xiabing. Stability of wire extension and arc length with GMA welding [J]. Transactions of the China Welding Institution, 1995, 16(2): 100-104.

作者简介: 段 彬,男,1982 年出生,博士,讲师. 主要从事数字焊接装备、可再生能源方向的科研和教学工作. 发表论文 10 余篇. Email: duanbin@sdu.edu.cn

通讯作者: 张承慧,男,教授. Email: zchui@sdu.edu.cn

Key words: wear resistance; microstructure; Fe-Cr-Ti-C alloy system

Modeling and simulation of pulsed welding inverter DU-AN Bin[1], ZHANG Chenghui[1], SUN Tongjing[1], ZHANG Guangxian[2], GUO Min[1] (1. School of Control Science and Engineering, Shandong University, Jinan 250061, China; 2. Shandong Aotai Electrical Co., Ltd., Jinan 250000, China). pp 57 - 60, 64

Abstract: The physical model including input and output rectifier filter, inverter and buck circuits was founded. According to actual parameters of every component, the modeling and simulation of the main loop circuit and digital control system were studied through the nonlinear interface model. Finally, the mathematical model of dynamic welding process was established to form the welding power source system model, and variation of physical quantities and dynamic response process were analyzed quantitatively. Simulation results predict the work process of the pulsed MIG welding power source, show the significance of welding current control and arc voltage control, which lay the foundation for further research.

Key words: welding inverter; pulsed welding; mathematical modeling; simulation

Welded joints fracture behavior of laser in-situ welding of high volume fraction SiC_p/2024 Al MMC LI Liqun[1,2], ZUO Zhicheng[1], TAO Wang[1], JIANG Longtao[3] (1. State Key Laboratory of Advanced Welding and Joining, Harbin Institute of Technology, Harbin 150001, China; 2. National Key Laboratory for Precision Hot Processing of Metals, Harbin Institute of Technology, Harbin 150001, China; 3. Metal Matrix Composites Institute, Harbin Institute of Technology, Harbin 150001, China). pp 61 - 64

Abstract: High volume fraction (45%) SiC_p/2024 aluminum matrix composite was jointed by laser in-situ welding method with a Ti foil as intermediate material, the welded joints fracture behavior under different welding conditions was compared in this paper. The results indicated that, the Ti foil intermediate thickness of 0.5 mm was more favorable to form sound bead appearance and interfaces morphology. The tensile strength of joints was up to 50% of the base materials when the fracture occured at the centre of weld, which was quasi-cleavage fracture mode. When the Ti foil intermediate thickness increased up to 0.8 mm, the weld was very susceptible to porosity, lack of fusion defects, and insufficient interfacial reaction, the fracture location always occured at the interface, the tensile strength was lower, which was brittle fracture mode.

Key words: aluminum matrix composites; titanium alloy; laser In-situ welding; fracture behavior

Microstructure and mechanical properties of friction stir welding joint of 7A05 aluminum alloy thick-sheet DONG Jihong, TONG Jianhua, GUO Xiaojuan, LUAN Guohong (Beijing Aeronautical Manufacturing Technology Research Institute, Aviation Industry Corporation of China, Beijing 100024, China). pp 65 - 68

Abstract: A new style stir head was designed to weld high strength aluminum alloy plate of 30mm thickness with friction stir welding. Microstructure and mechanical properties of friction stir welded joint of 7A05-T6 aluminum alloy thick plate were investigated. The results show that the dynamic recrystallization takes place in the weld nugget zone and fine grains are formed. Regarding to the thermo-mechanically affected zone on the sides, the advancing side consists of narrow slate grains, while the retreating side consists of flat and nubby grains. The adjusting range of process parameters is very narrow for welding of 30mm plate. When the rotating speed was 360 r/min and welding speed was 120 mm/min, the defect-free weld with good appearance was obtained, and the tensile strength of the weld reached 367.7 MPa, yield strength reached 280.8 MPa and the elongation reached 14.4%. Tensile strength of the weld could reach up to 95% of the base metal, and the elongation was higher than that of the base metal.

Key words: friction stir welding; mechanical properties; microstructure

Control algorithm of torch posture for plasma cutting of welding groove along multi-pipe intersecting edge TIAN Guohua[1], OU Changjin[2], HUANG Dechao[1] (1. Xiaoshan College, Zhejiang Radio & TV University, Hangzhou 311200, China; 2. College of Mechanical Engineering, Zhejiang University of Technology, Hangzhou 310014, China). pp 69 - 72

Abstract: In order to ensure the proper cutting and improve the cutting efficiency of welding groove along multi-pipe intersecting as well, by setting up a mathematic mode on the multi-pipe consistency, It is then puts forward the control algorithm of torch posture for NC cutting of welding groove along multi-pope intersecting edge. The discrete algorithm of torch posture on the basis of plasma cutting characteristics was put forward, which discreted the control algorithm of welding groove along multi-pope intersecting, the result of discretion was also given. The change of cutting speed was stimulated with MATLAB, and finally the experiment of cutting was carried out based on the control algorithm of the posture. Theoretical analysis and simulation result showed that the algorithms could disporse the torch posture efficiently based on the cutting thickness, achieve the precise control of cutting speed based on the characteristics of plasma cutting, hence, it could improve cutting quality effectively.

Key words: plasma cutting; intersection curve; torch posture; algorithm

Special tin whisker growth on surface of oxidized RE-phases TIAN Jun[1], LI Dongnan[1], LI Wei[1], HAO Hu[2] (1. Department of Materials Science and Engineering, Fujian University of Technology, Fuzhou 350108, China; 2. College of Mechanical Engineering and Applied Electronics Technology, Beijing University of Technology, Beijing 100124, China). pp 73 - 76

Abstract: $CeSn_3$ and $ErSn_3$ phases with large size were precipitated in the Sn-3.8Ag-0.7Cu-1.0Ce/Er solder alloys. The aging treatment at room temperature and 150℃ was carried out for the prepared sample of Sn-3.8Ag-0.7Cu-1.0Ce/Er solder alloy, respectively. After various storage periods, the tin whiskers appeared on the specimen surfaces were analyzed by scanning electron microscopy (SEM). The results indicated that a great